MIJST
MIST International Journal of Science and Technology

Development of a Probabilistic Correlation between the Gamma Ray Index and Shale Volume Factor to Improve Resource Estimation for the Niger Delta Basin, Nigeria

Judith O. George[1,3], Olalere Oloruntobi[2], and Stephen D. Butt[1*]

[1]Department of Process Engineering, Memorial University of Newfoundland, St. John's, Canada
[2] Strata Well Services Limited, Benin, Nigeria
[3]Department of Wells, Shell Petroleum Development Company, Port Harcourt, Nigeria

emails: [1]*jogeorge@mun.ca; [2]oso866@mun.ca; and [*1]sdbutt@mun.ca*

ARTICLE INFO

Article History:

Received: 26th May 2024
Revised: 10th June 2024
Accepted: 19th June 2024
Published: 30th June 2024

Keywords:

Shale volume factor
Gamma Ray Index
X-Ray Diffraction
Cores
Gamma Ray Logs

ABSTRACT

The shale volume factor is among the critical petrophysical parameters for reservoir characterization and formation evaluation. Inaccurate estimates of the shale volume factor can lead to poor reserves or resource estimates and wrong business decisions. While the current industry standard is to estimate the shale volume factor from the gamma ray logs using the concept of the gamma ray index, a relationship between the shale volume factor and the gamma-ray index needs to be established for any region/basin under consideration. For most applications in the Niger Delta Basin, a linear relationship is often assumed. However, there is no proven relationship between the shale volume factor and the gamma-ray index for the formations in the Niger Delta Basin. This paper proposes a new shale volume factor prediction correlation for the Niger Delta Basin in Nigeria. The correlation development is based on establishing a relationship between the shale volume factor obtained from cores and the gamma ray index obtained from petrophysical logs for over thirty wells drilled across the Niger Delta Basin. The results show that the relationship between the shale volume factor and the gamma-ray index is not linear as often assumed but a power law model. The new probabilistic correlation predicts lower shale volume factors than the linear model for all ranges of the gamma-ray index. This recent correlation will significantly impact how the hydrocarbon resources and reserves are quantified in the Niger Delta Basin.

1. INTRODUCTION

Accurate knowledge of the shale volume factor is required for petrophysical evaluations and hydrocarbon reserve estimates and impacts the determination of several key parameters such porosity, density, compressional wave velocity, permeability and hydrocarbon saturation. For liquid-filled non-clean rocks, effective porosity can be expressed as functions of rock matrix density, shale matrix density, saturating fluid density, formation bulk density, and shale volume factor as presented by (Oloruntobi & Butt, 2019) in Equation 1.

$$\emptyset = \left[\frac{\rho_{ma}}{\rho_{ma}-\rho_{fl}}\right] - \left[\frac{1}{\rho_{ma}-\rho_{fl}}\right]\rho_b - \left[\frac{\rho_{ma}-\rho_{sh}}{\rho_{ma}-\rho_{fl}}\right]V_{sh} \quad (1)$$

In regions where density logs are unavailable, accurate knowledge of the shale volume factor is required to generate the pseudo-density log for overburden gradient computation. Oloruntobi & Butt (2019) showed that the formation bulk density depends on compressional velocity and shale volume factor shale volume factor for siliciclastic formations. Equation 2 which applies to sedimentary rock is an adaptation of the Birch (1961) model; an empirical relationship for computing the bulk density for igneous and metamorphic rocks.

To expand the original Birch (1961) model and ensure its applicability to sedimentary rocks, the results of the experimental ultrasonic tests that Hans et al. (1986) conducted on brine saturated-sandstone core samples were used. These tests furnished the values of formation properties (compressional wave velocity, shale volume an+d formation bulk density) which were very beneficial in extending the use of Birch (1961) model to shaly

siliciclastic sedimentary rocks. This update is reflected in Equation 2.

$$\rho_b = 0.222V_p + 0.361V_{sh} + 1.431 \quad (2)$$

Equation 3 is also an extension of another earlier model by Gardner et. al. (1974) and further updates which were predominantly beneficial in determining the bulk density of consolidated and water-saturated rock under significant effective stress. With Equation 3, the formation bulk density of sandstones, shales and shaly sands can be estimated.

$$\rho_b = 1.350\left[V_p + 1.651V_{sh}\right]^{0.390} \quad (3)$$

Yusuf et al. (2019) extended the work of Oloruntobi and Butt (2019) for intact and fractured siliciclastic rocks and showed the dependency of formation bulk density on compressional velocity, shear velocity, and shale volume factor. This relationship is evident in Equation 4:

$$\rho_b = 1.859\left[V_p - V_s + 0.205V_{sh}\right]^{0.503} \quad (4)$$

The shale volume factor must be known along with porosity to be able to derive compressional velocity empirically (Kowallis et al., 1984; Castagna et al., 1985; Han et al., 1986; Eberhart-Phillips et al., 1989; Xu & White, 1995) using the general relationship in Equation 5:

$$V_p = A - B\emptyset - CV_{sh} \quad (5)$$

The shale volume factor is a critical consideration in evaluating the permeability of a fluid-filled sandstone reservoir. Shale reduces the permeability of the reservoir by either causing bridging across two sand bodies (laminated shale) or causing narrowing of the pore throats of the sand (dispersed shale). Schön (2015) quantitatively articulated the impact of shale volume factor on the vertical and horizontal permeabilities of laminated shaly sand as represented in Equation 6:

$$k_v = \left(\frac{1-V_{sh}}{k_{sd}} + \frac{V_{sh}}{k_{sh}}\right)^{-1} ; k_h = (1 - V_{sh}).k_{sd} + V_{sh}.k_{sh} \quad (6)$$

Other models that relate reservoir porosity and permeability to the shale volume factor are outlined in Table 1. Finally, the presence of shale in sandstone reservoirs introduces an extra component of electrical conductivity (Winsauer & McCardell, 1953).Thus, a formal application of Archie's equation without accounting for the influence of shale volume factor will lead to an overestimation of reservoir water saturation. The impact of shale volume factor on the saturation of non-clean sand is shown in Table 2.

Table 1
Models for Calculating Porosity and Permeability of Dispersed Shale (Schön, 2015)

Model	Equation
Revil & Cathles (1999)	$\emptyset = \emptyset_{sd} - V_c(1 - \emptyset_{sh})$
	$k = k_{sd}\left[1 - V_c\left(\frac{1-\emptyset_{sh}}{\emptyset_{sd}}\right)\right]^{3m_{cs}}$
Schon & Georgi (2003)	$k_{shaly\ sand} = k_{sand}\left(1 - \alpha.\frac{V_{sh}}{\emptyset}\right)^2$

Table 2
Models to Compute Saturation of Water-Saturated Shaly Sandstone Reservoir

Model	Equation
Poupon et al., (1954) N.B. For laminated shale	$\frac{1}{R_t} = \frac{1 - V_{sh}}{R_{sd}} + \frac{V_{sh}}{R_{sh}}$ $\frac{1}{R_t} = \frac{1 - V_{sh}}{R_{sd}}.(\emptyset^m - S_w^n) + \frac{V_{sh}}{R_{sh}}$ $S_w = \left[R_w.\left(\frac{1}{R_t} - \frac{V_{sh}}{R_{sh}}\right).\frac{1}{\emptyset^m}.\frac{1}{1-V_{sh}}\right]^{1/n}$
Simandoux Equation (Simandoux, 1963) and modified by (Bardon & Pied, 1969) N.B. Based on artificially composed materials (sand and clay) and representing the structural and dispersed type of shale distribution in a reservoir	$C_t = \frac{\emptyset^m}{a.R_w}S_w^n + V_{sh}.C_{sh}.S_w$ When n=2, water saturation is shown below $S_w = \frac{1}{2} * \frac{R_w}{\emptyset^m}\left[\sqrt{4 * \frac{\emptyset^m}{R_w.R_t} + \left(\frac{V_{sh}}{R_{sh}}\right)^2} - \frac{V_{sh}}{R_{sh}}\right]$
Indonesian Equation (Poupon & Levaux, 1971) Recommended for shaly formations with relative freshwater	$C_t = \frac{C_w}{F}.S_w^2 + 2\sqrt{\frac{C_w - C_{shale}}{F}.V_{shale}^{2-Vsh}.S_w^2 + V_{shale}^{2-Vshale}.C_{shale}.S_w^2}$ When Vsh <= 0.5, the simplified form of the equation is $C_t = \frac{C_w}{F}.S_w^2 + 2\sqrt{\frac{C_w - C_{shale}}{F}.V_{shale}.S_w^2 + V_{shale}.C_{shale}.S_w^2}$

In general, the best method of determining the shale volume factor is to experimentally conduct X-ray Diffraction on core samples obtained from undisturbed reservoirs (Barba & Allen, 2001; McPhee et al., 2015; Schön, 2015; Prasse et al., 2019). However, coring may be expensive and hazardous, and acquiring cores at every desired depth is practically impossible. Although the rock cuttings obtained during drilling can provide samples of subsurface rocks, they are of limited use in formation properties evaluation noting that Serra (1984) highlighted that these cuttings had experienced mixing, leaching, and contamination while being circulated in the drilling fluid from the bit to the surface. Given these limitations, well logging is an effective alternative for taking in-situ reservoir properties measurements. Empirical correlations have been developed to estimate the shale volume factor from petrophysical properties typically relating log-derived data (gamma ray index - I_{GR}) to the shale volume factor.

Several researchers have developed correlations between gamma-ray reading and shale volume factor. Equation 7 is a linear correlation between gamma ray reading and shale volume (André Poupon & Gaymard 1970). This relationship was derived from statistical evaluation. It holds for a constant radioactive level of clay, provided no other mineral in the formation contributes to the radioactivity measurements.

$$V_c = V_{sh} = I_{GR} = \frac{GR_{log} - GR_{min}}{GR_{max} - GR_{min}} \quad (7)$$

Despite the difference between the shale volume and the clay volume (Bhuyan & Passey, 1994; Kennedy, 2021; Prasse et al., 2019), Equation 7 has been used to estimate the shale volume from the gamma-ray log (Oloruntobi & Butt, 2019; Kennedy, 2021). Notwithstanding the extensive application of the linear correlation in shale volume estimation, its use can lead to an erroneous prediction of shale volume (Prasse et al., 2019).

Larionov (1969) proposed two nonlinear equations showing the dependency of the shale volume factor on the gamma ray index (one applies to young rocks while the other applies to older rocks). These relationships were developed from experimental data and are based on the premise that shales contain 90% clay and were initially published as nomographs (Prasse et al., 2019; Kennedy, 2021). Equation 8 is the relationship that Larionov (1969) derived for young rocks - Mesozoic and Tertiary rocks in the southern area of the U.S.S.R.

$$V_{shale} = 0.083 * (2^{3.7 I_{GR}} - 1) \quad (8)$$

While for older rocks – Paleozoic rocks in the Urals and European parts of the USSR, Larionov (1969) presented Equation 9.

$$V_{shale} = 0.33 * (2^{2 I_{GR}} - 1) \quad (9)$$

Equations 7-9 have been widely applied in shale volume factor estimation for later studies (e.g. Essien, 2019; Szabó, 2011; Oyeyemi et al., 2019; Kennedy, 2021).

Equation 10 represents the nonlinear empirical correlation developed by Stieber (1970) using log data from wells drilled in the Tertiary sediments of the Louisiana Gulf Coast.

$$V_{shale} = \frac{I_{GR}}{3 - 2 I_{GR}} \quad (10)$$

Several authors have since used Stieber's equation to estimate shale volume including Prasse et al. (2019). The main limitation of this relationship is that even though it was developed through a statistical approach, it was not calibrated with actual measurements of shale volume from cores (Prasse et al., 2019; Stieber, 1970).

Clavier et al. (1971) showed a relationship between volume of shale and gamma ray index. Figure 1 is the original nonlinear curve describing this connection and which was later represented as the empirical correlation.

This non-linear plot was transformed over time into a mathematical relationship:

$$V_{sh} = 1.7 - \sqrt{3.38 - (I_{GR} + 0.7)^2} \quad (11)$$

This model has also been used to estimate the shale volume factor (Fajana, 2021). However, its main limitation, like Stieber (1970), is that it has not been calibrated with actual measurements of shale volume from core samples (Prasse et al., 2019).

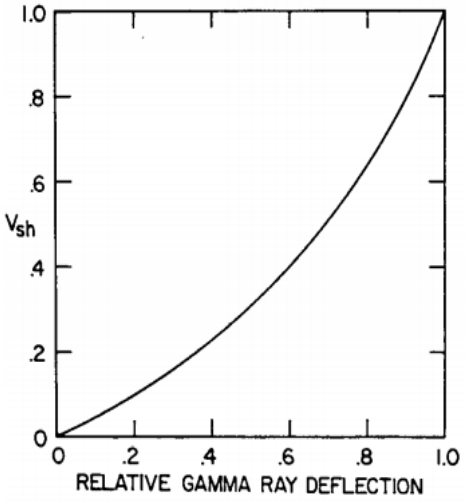

Figure 1: Clavier's Model Presented as a Curve (Clavier et al. 1971)

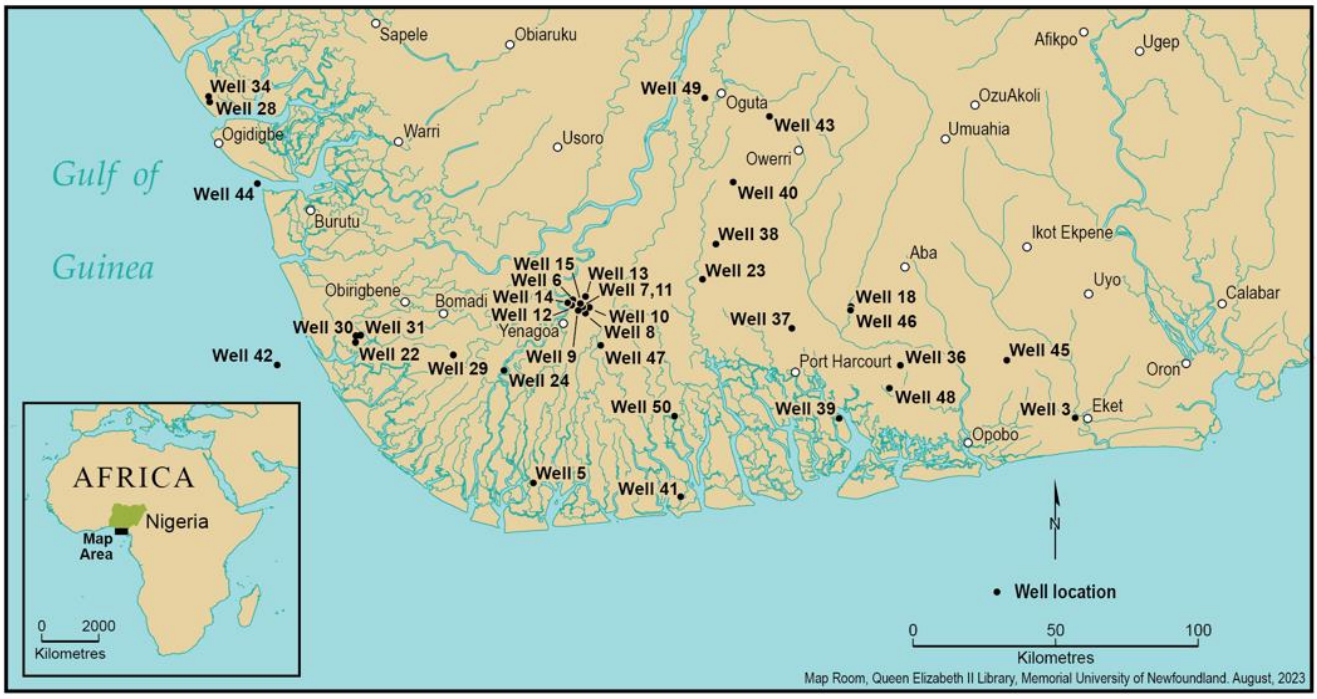

Figure 2: Location Map showing all the wells considered for the development of the Correlation.

For shale volume estimation from the gamma-ray log in the Niger Delta Basin, use has been made of linear, Stieber's, Clavier's, and Larionov's relationships (Oyeyemi et al., 2019; Essien, 2019; Oloruntobi & Butt 2020; Fajana, 2021). However, none of these models have been developed using data for the Niger Delta Basin and no studies have been done to evaluate their accuracy for this basin or to derive new corelations based on data from the basin.

Therefore, the objective of this work is to develop a core-derived correlation that will be used to obtain accurate shale volume factor from log-derived Gamma Ray Index specifically for the Niger Delta Basin. This is especially important since acquiring cores and the associated Special Core Analysis can be hazardous and expensive, leading to more routine use of gamma ray logs for shale volume derivation. This technical paper utilizes the results of 92 whole rock and clay mineralogy analyses conducted on cores obtained from 34 oil and natural gas wells in the Niger Delta Basin and the associated well logs.

2. FIELD DATA

With the beginning of hydrocarbon exploration in Nigeria, there was a significant need to understand the coastal sedimentary Niger Delta Basin (Short & Stauble, 1967). Following the work of many workers in the region, in-depth knowledge of the basin has been gained and published (Adewole et al., 2016; Avbovbo, 1978; Daukoru, 1975; Doust, 1990; Doust & Omatsola, 1990; Evamy et al., 1978; Short & Stauble, 1967; Tuttle et al., 1999). The Niger Delta Basin, located in the Gulf of Guinea, is an extensional basin formed due to rifting at the Atlantic Ocean (Adewole et al., 2016; Oloruntobi et al., 2020). The basin covers about 75,000 km^2 and has clastic sedimentary deposits whose thicknesses range from 9,000 m to 12,000 m (Evamy et al., 1978). Growth faults and rollover anticlines are key structural traps in the basin (Daukoru, 1975; Oloruntobi & Butt, 2019c).

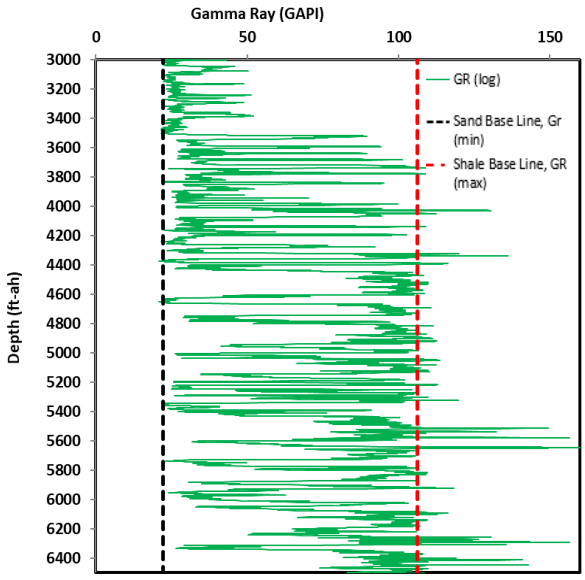

Figure 3: Determination of Gamma Ray Index from GR Log

In decreasing depth, three significant formations in the basin are Akata, Agbada, and Benin Formations (Avbovbo, 1978; Oloruntobi & Butt, 2019c). The Benin formation as mostly freshwater-containing braided river systems sandstones with high porosity (Avbovbo, 1978) containing predominantly quartz and potash feldspar with trace amounts of plagioclase. The formation consists of a sandstone-shale sequence with a thickness up to a maximum of about 4000 m. The sandstones in the Agbada formation are similar in origin and composition as the

Benin Formation sandstones. The Akata formation consists mostly of under-compacted and sometimes over pressured siltstone and sandstones (Avbovbo, 1978). The crude oil generated in the Akata formation is believed to have possibly migrated upwards through growth faults in the basin before accumulating in the Agbada formation (Adewole et al., 2016; Avbovbo, 1978). Shales through the basin contain kaolinite (about 75%) and mixed amounts of illite and montmorillonite.

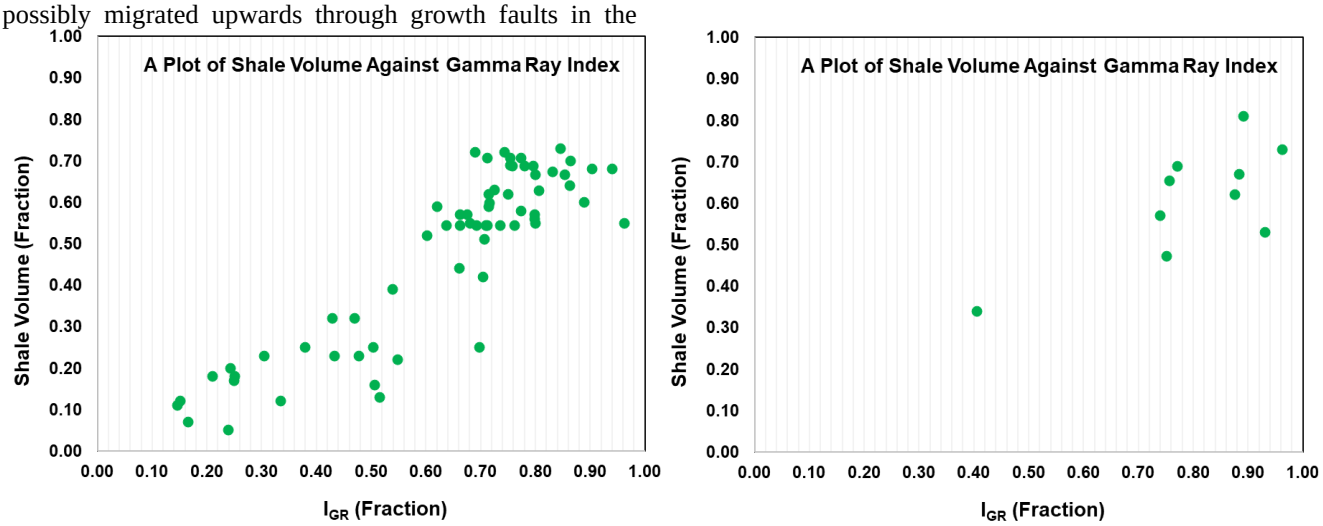

Figure 4: Plots of Shale Volume against Gamma Ray Index where kaolinite is the dominant clay mineral (left) and chlorite is the dominant clay mineral (right).

Figure 2 shows the location map for the wells used to develop this new shale volume prediction correlation. Table A-1 in Appendix A provides a summary of the well data which includes 92 Shale Volume Data and Gamma-Ray Indices at different depths from 34 wells located all over the basin across the land and swamp fields. The well data used to prepare this correlation cover a range of depths from 4,609 ftah to 15729 ftah. For data analyses in this study, all depths used are Measured Depths along the hole. The shale volumes were measured through X-ray Diffraction conducted on the cores while the Gamma-Ray Indexes were computed from gamma-ray logs. The XRD results show the whole rock composition as well as the mineralogy of the contained shale. The depth of the core (used to derive the shale volume) matched the depth of the gamma ray reading (used for calculating the gamma ray index).

The dominant clay mineral in the studied wells is kaolinite, as seen in Table B-1 of Appendix B. The average kaolinite content across the wells is 61.2% (dominantly occurring in 77 cores across 34 wells). In comparison, chlorite constitutes 13% of the clay minerals (dominantly occurring in 11 cores across 7 wells). In most cases, kaolinite and chlorite were seen to be two major clay mineral constituents. The average composition of other clay minerals identified in the cores are mica (7.5%), mica-smectite (5.1%), smectite (1.4%), vermiculite (0.1%), illite (0.3%), mica-vermiculites (5.4%), illite/mica (1.6%), chlorite/mica (0.5%), chlorite smectite (0.5%), and illite/smectite (3.4%). Table B-2 in Appendix B provides the summary of the clay mineral composition of the core samples.

3. DEVELOPMENT OF CORRELATION

To establish a relationship between the Gamma Ray Index and the actual volume of shale, core samples and gamma ray logs were taken at several depths across 34 wells. To establish the correlation, core samples were acquired from pre-determined depths along the well paths. X-ray Diffraction (XRD) was carried out on these core samples to provide both qualitative and quantitative analyses on whole rock mineralogy and clay mineral composition (Hanawalt et al., 1986; Ramachandran & Beaudoin, 2000) with results given in Tables 5 and 6 in Appendix 1.

Gamma Ray logs were then acquired from corresponding 34 wells as given in Appendix 1. For each log, the shale base line and sand baselines were determined. Shale baseline is a line drawn to correspond to gamma ray reading in wholly shale interval while sand baseline is a line drawn to align with the gamma ray response in clean sand interval in the well path. An example for the log analysis is shown in Figure 3. In the absence of Neutron and Density logs, the Gamma Ray logs can be used to compute the Gamma Ray Index, which is sometimes used as volume of shale. Gamma ray of clean sandstone is defined as the 5th percentile of entire population of gamma ray readings obtained in the logged interval while the gamma ray value of shale is defined as 95th percentile of the logged gamma ray readings. Sayers and den Boer (2021) pointed out that clean sandstones have been understood to be sandstones whose shale volume fraction is less than 0.05. From the gamma ray data, the Gamma Ray Index (I_{GR}) is computed for readings at each depth along the well path using the relationship from Equation 7.

At this Table A-1 in Appendix B lists the results of the shale volumes from XRD analysis and the calculated Gamma Ray Index at different depths across various wells. Figure 4 shows the corresponding plots of Vsh versus I_{GR}. At this stage of the core data analysis, shale volume data where kaolinite is the main clay mineral constituent are evaluated separately from data where chlorite is the main clay mineral because of the likely differing origins of these shales and potentially different correlations. Kaolinite and chlorite are two types of clay minerals. Miranda-Trevino and Coles (2003) described the structure of kaolinite,

highlighting its stability and non-swelling nature.

Pauling, L. (1930) had also earlier provided information on the key structural difference between chlorite and kaolinite. Cheng and Heidari (2017) also pointed out that the major indication of the structural difference between these minerals is the resultant reactivity of each mineral Cation Exchange Capacity (CEC). CEC, which represents the quantity of exchangeable cations of each clay mineral, is a measure of the reactivity of the individual mineral.

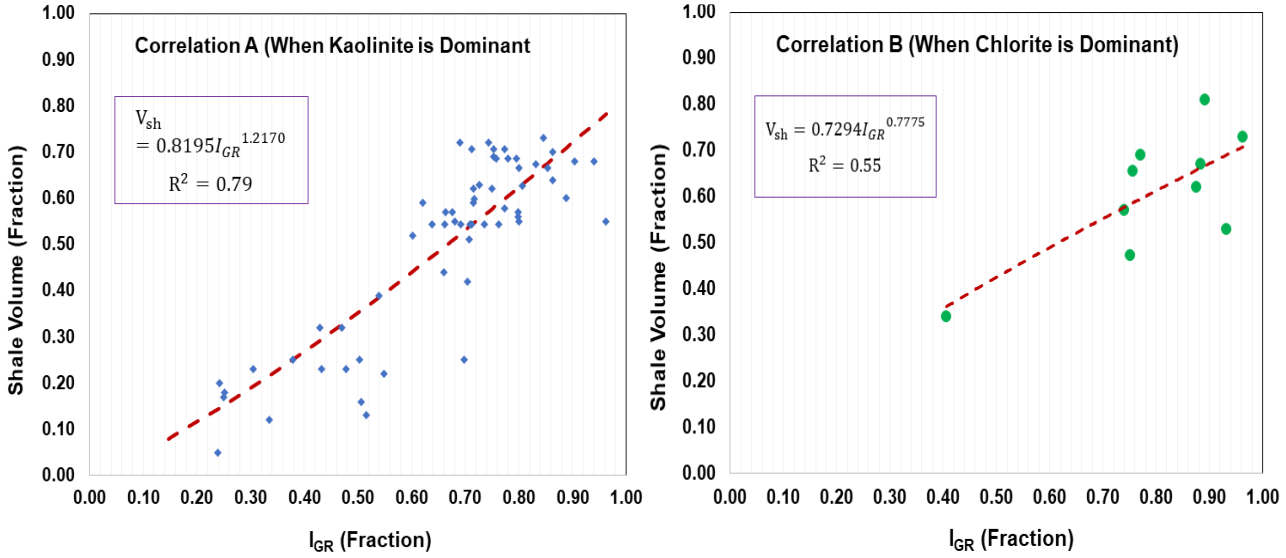

Figure 5: Correlations A and B between Shale Volume and Gamma Ray Index for dominantly kaolinite (left) and dominantly chlorite (right)

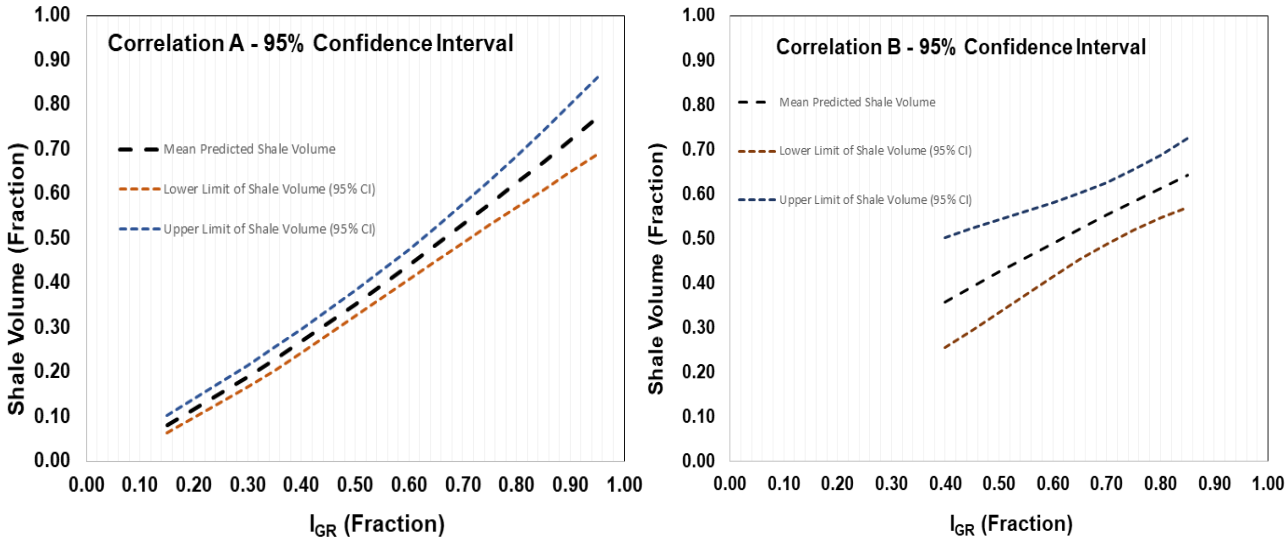

Figure 6: 95% Confidence Interval for Shale Volume Predicted with both correlations.

While chlorite is largely unreactive with a reported CEC lying between 10-40, kaolinite is the most unreactive and stable of the shale minerals with CEC between 3-15. Typically, distinction between kaolinite and chlorite in sediments can be achieved through X-ray diffraction on acquired core samples (Biscaye 1964; Elverhøi and Rønningsland 1978). However, a recent study shows that a crossplot between photoelectric effects (obtained from photoelectric logs) and the Thorium/potassium ratio obtained from spectral gamma ray log can shows a clear difference between kaolinite and chlorite (Al-Jafar and Al-Jaberi 2022).

Equation 12 is the best-fit correlation:

$$\text{Minimum} \sum_{i-1}^{n} [V_{sh}(\text{measured}) - V_{sh}(\text{predicted})]^2 \qquad (12)$$

These analyses showed that a power model best describes the relationship between the shale volume acquired from core samples and the calculated Gamma Ray Index.

Correlation A represents the cores whose main clay mineral constituent is kaolinite and was developed with 65 data pairs, whereas Correlation B represents the cores with chlorite is the main clay mineral content and was developed with 10 pairs of data. Due to inherent scatter of the data, the coefficient of correlation (a statistical measure

of the dependence of shale volume on gamma ray index, R^2) are 0.79 for Correlation A and is of 0.55 for Correlation B.

Figure 5 shows the results of the regression analyses with the Correlation A given in Equation 13:

$$V_{sh} = 0.8195 * I_{GR}^{1.2170} \quad (13)$$

and for Correlation B given as:

$$V_{sh} = 0.7294 * I_{GR}^{0.7775} \quad (14)$$

The deterministic empirical correlations resulting from regression analysis yields the predicted mean value of the dependent variable (Alfredo & Tang, 2007). As such, it is critical to compute the confidence interval of the empirical model to establish the possible range of the predicted dependent values. When the regression coefficients are estimated from a finite sample with several elements (η), their underlying probability distribution function is the t-distribution, whose degree of freedom is (η-2) (Alfredo & Tang, 2007).

Hence, the mean value of the dependent value estimated from the empirical model will have an underlying t-distribution with (η-2) degrees of freedom. There is no definitive information about the accuracy of the empirical modelling when considering the randomness underlying the independent variables. However, it has been demonstrated that the accuracy of an empirical model improves with increasing number of plotted data points (Alfredo & Tang, 2007).

Hypothesis testing is a quantitative measurement of the accuracy of each estimated dependent variable. First, a hypothesis (a statement about the parameter of the sample population, here the value of the estimated dependent variable) is defined. Next, the suitable test statistic and its underlying probability distribution is shown. Subsequently, the test statistic is estimated. As the test statistic is a random variable, there is a probability of error in estimating its value from a sample of finite size. One mostly considered error type is Type I error. The probability of a Type I error (rejecting a null hypothesis when it is true) is the level of significance (α) and its specification is one of the steps of hypothesis testing (Alfredo & Tang, 2007). In practice, typical values of level of significance lie between 1% and 5%. Finally, the unacceptable region (within which the null hypothesis is rejected) is specified.

In this study, the selected level of significance is 5% and the associated confidence interval is 95%. Using this basis for computing (1- α) confidence interval for the empirical models at selected values of the dependent variable, the lower limit of the confidence interval is given by Equation 15.

$$\langle \mu_{Y/x_i} \rangle_{1-\alpha} = \bar{y_i} - t_{\left(1-\frac{\alpha}{2}\right),(\eta-2)} . S_{Y/x} . \sqrt{\frac{1}{\eta} + \frac{(x_i - \bar{x})^2}{\Sigma (x_i - \bar{x})^2}} \quad (15)$$

and the upper limit given in Equation 16:

$$\langle \mu_{Y/x_i} \rangle_{1-\alpha} = \bar{y_i} + t_{\left(1-\frac{\alpha}{2}\right),(\eta-2)} . S_{Y/x} . \sqrt{\frac{1}{\eta} + \frac{(x_i - \bar{x})^2}{\Sigma (x_i - \bar{x})^2}} \quad (16)$$

Where Equation 17 computes the conditional standard deviation:

$$S_{Y/x} = \sqrt{\frac{(y_i - y_{estimated})^2}{n-2}} \quad (17)$$

Figures 6 shows the resulting 95% confidence intervals for Correlations A and B. The confidence interval for Correlation B is wider because of the greater uncertainty introduced in developing the model with limited number of data as is shown by the value of the test statistic.

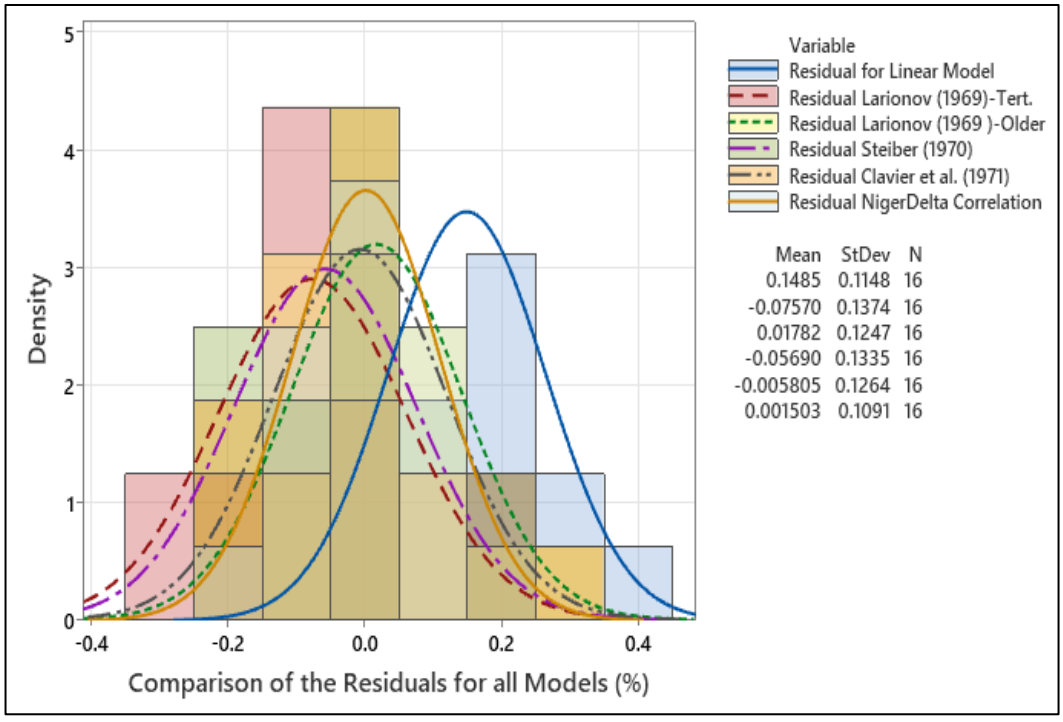

Figure 7: Histograms of residuals for all 5 existing models and the new Niger Delta Correlation.

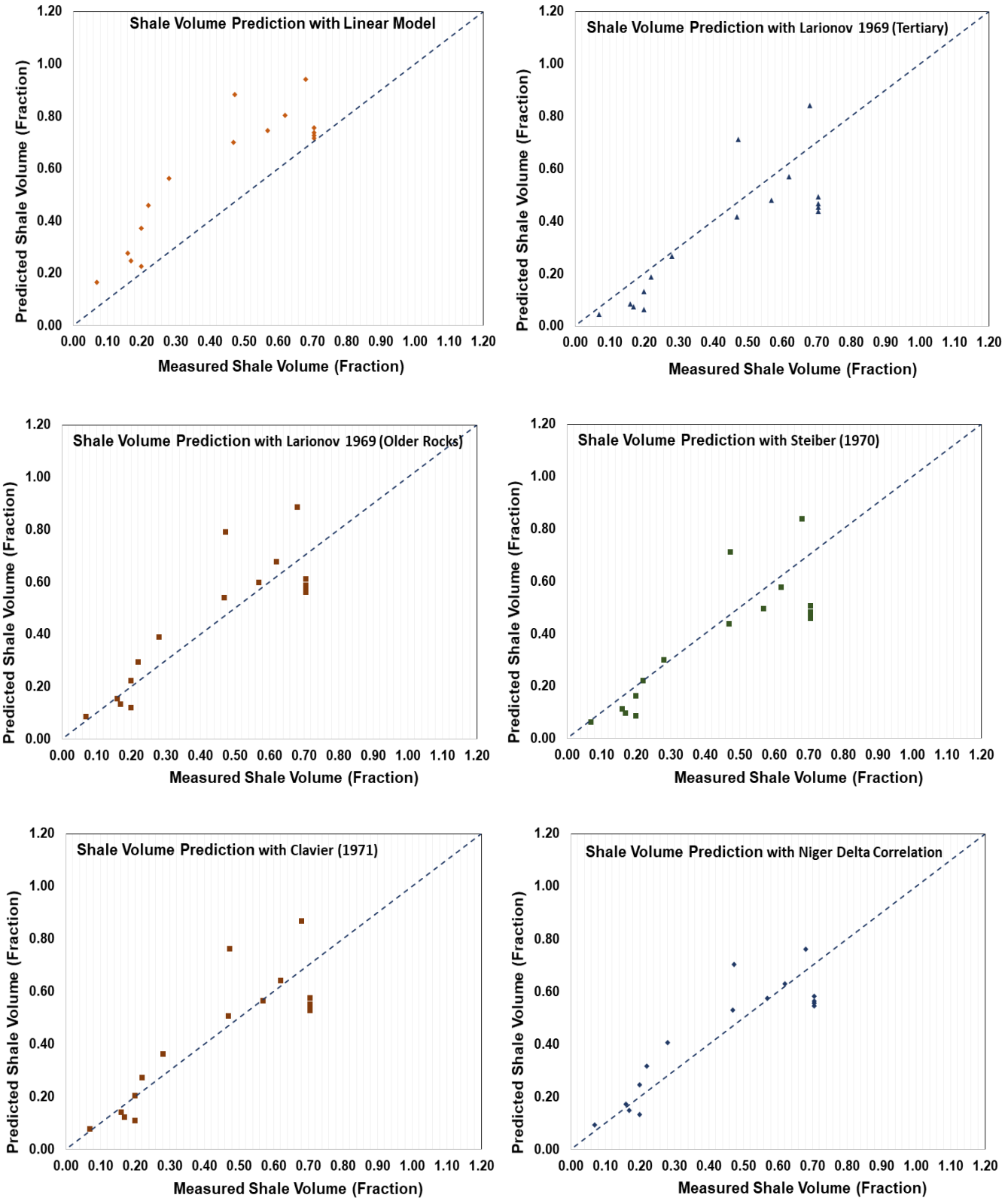

Figure 8: Plots of accuracy and bias associated with the shale volume predicted with the 5 existing models evaluated in this study and the new Niger Delta Correlation.

Both linear and nonlinear regression analyses were then conducted to develop the correlations between Gamma Ray Index and Shale Volume, with the suitability test of each correlation being done using the method of the last squares. The best-fit correlation is such that the sum of the square of the residual values (the difference between the measured shale volume and the predicted shale volume) is minimum.

Equations 13 and 14 shows that a corresponding shale volume of 0 is forecast at the zero value of the gamma ray

index. On the other hand, the predicted value of the shale volume when the gamma-ray index is 0.786. Equation 13 is quite different from the linear model widely used in the Niger Delta which posits that the actual shale volume equals the gamma-ray index computed from the gamma-ray readings. The following section develops the methodology to validate the newly formulated Niger Delta power-law model correlations and compares with the existing models discussed in the introduction (Clavier et al., 1971; Larionov, 1969; Stieber, 1970).

4. VALIDATION OF CORRELATION

16 pairs of data were used to validate Correlation A with only one pair available for Correlation B as indicated in Appendix A. Therefore, this section focuses on validating Correlation A. Figures 7 plots the predicted Shale Volume Fraction versus the core measurements for the 5 previously described models and the new Power-Law Correlation. Data points that fall along the dashed line with a slope of 1 indicate a perfect prediction while data that plot above the line indicate an over-estimation and data plotting below the line show an under-estimation.

Therefore, the slope of the least squares linear regression is representative of the bias of the estimation model with slopes greater than 1 indicating an over-estimation bias and vice versa. Visual analysis of these plots indicates a strong overestimation bias for the Linear Model, with no clear bias for the other 5 models. Further analysis of the accuracy and bias is done by analysis of the histogram distribution of residual. Equation 18 is used to calculate the difference between the predicted and actual shale volume measurements using:

$$Residual = Predicted\ Vsh - Actual\ Vsh \qquad (18)$$

Using this methodology, the standard deviation of the residuals is representative of the accuracy of the estimation models and the mean value is representative of the bias. Figure 8 plots the histograms of residuals for the 5 previously described models and the new Power-Law Correlation along with the corresponding standard deviations and means values. These results show that the linear model overpredicts shale volume for every considered instance and is consistent with the data shown in Figure 7. The Larionov (1969) model for young rocks (Tertiary and younger) and the Steiber (1970) model both under-predict the shale volume in most instances with mean residual values less than one. The Larionov (1969) model for older rocks and the Clavier (1971) model resulted in more accurate and less biased predictions based on the smaller standard deviations and mean values closer to 1. Finally, the new Niger Basin Correlation has the lowest standard deviation and mean closest to 1, indicating the most accurate and least biased of estimation models.

Finally, the estimation accuracy of the 6 models was examined by determination of the Root Mean Square Error (RMSE) a measure of the mean of the square of the residuals, with lower RMSE values indicating greater accuracy. These are given in Table 3, which agrees with the data in Figure 8. These results show that the most accurate relationship for shale volume prediction in the Niger Delta Basin is the new correlation with the Clavier (1971) model and the Larionov (1969) model for older rocks also providing close estimations. With the probabilistic approach shown earlier, the 95% confidence intervals for mean shale volumes predicted with the new Niger Delta shale volume correlation will be obtained.

Table 3

Root Mean Square Error (RMSE)

MODEL	RMSE
Linear Model (Equation 10)	0.186
Larionov (1969) - Tertiary Rocks	0.153
Larionov (1969) - Older Rocks	0.122
Steiber (1970)	0.141
Clavier et al. (1971)	0.123
Niger Delta Correlation (Power Law)	**0.106**

5. CONCLUSION

A new probabilistic shale volume prediction correlation has been developed using shale volume XRD core measurements and corresponding gamma ray log readings from wells in the Niger Delta Basin. Both land and swamp sections of the basin were covered by the model. This is the first model which uses actual measured shale volume and gamma ray readings from the Niger Delta Basin to develop a relationship for predicting shale volume using gamma ray index. This proposed model can find wide application when: (1) there are limited opportunities to acquire core samples and measure actual shale volume using X-ray Diffraction; and (2) there is limited budget to acquire additional well logs only gamma ray logs are available for shale volume computation. This correlation is quite applicable as most operators routinely have the acquisition of gamma ray logs in the logging programs (especially as gamma ray tools do not require nuclear sources). Although this correlation was developed with well data from the Niger Delta Basin, it can find important application for shale volume prediction in other basins around the world as it has compared favourably to other existing models.

DECLARATION OF COMPETING INTEREST

The authors declare that they have no known personal relationships or competing financial interests that influenced or could have appeared to influence the work reported in this paper.

ACKNOWLEDGEMENT

The well data utilized for this study were obtained from Shell Petroleum Development Company, Port Harcourt, Nigeria through the Department of Petroleum Resources, Nigeria. The authors sincerely thank these organizations for their support and collaboration.

REFERENCES

Adewole, E. O., Macdonald, D. I. M., & Healy, D. (2016). Estimating density and vertical stress magnitudes using hydrocarbon exploration data in the onshore Northern Niger Delta Basin, Nigeria: Implication for overpressure prediction. *Journal of African Earth Sciences*, *123*, 294–308. https://doi.org/10.1016/j.jafrearsci.2016.07.009

Alfredo, H., & TANG, W. H. (2007). Probability concepts in engineering. *Planning*, *1*(4), 1–3.

Al-Jafar, M. K., & Al-Jaberi, M. H. (2022). Determination of clay minerals using gamma ray spectroscopy for the Zubair Formation in Southern Iraq. *Journal of Petroleum Exploration and Production Technology*, 1–8.

Avbovbo, A. A. (1978). Tertiary lithostratigraphy of the Niger Delta. *AAPG Bulletin*, *62*(2), 295–306.

Barba, R. E., & Allen, M. P. (2001). Development and Validation of an Integrated Reservoir Pressure and Effective Gas Permeability Model Using Wireline Log and Pre-Frac Pump-in Test Data in the Bob West Field, South Texas Wilcox. *SPE Annual Technical Conference and Exhibition*.

Bardon, C., & Pied, B. (1969). Formation water saturation in shaly sands. *SPWLA 10th Annual Logging Symposium*.

Bhuyan, K., & Passey, Q. R. (1994). Clay estimation from GR and neutron-density porosity logs. *SPWLA 35th Annual Logging Symposium*.

Birch, F. (1960). The velocity of compressional waves in rocks to 10 kilobars: 1. *Journal of Geophysical Research*, *65*(4), 1083–1102.

Biscaye, P. E. (1964). Distinction between kaolinite and chlorite in recent sediments by X-ray diffraction. *American Mineralogist: Journal of Earth and Planetary Materials*, *49*(9–10), 1281–1289.

Castagna, J. P., Batzle, M. L., & Eastwood, R. L. (1985). Relationships between compressional-wave and shear-wave velocities in clastic silicate rocks. *Geophysics*, *50*(4), 571–581.

Cheng, K., & Heidari, Z. (2017). A new method for quantifying cation exchange capacity in clay minerals. *SPWLA Annual Logging Symposium*, D053S017R002.

CLAVIER C, HOYLE W, & MEUNIER D. (1971). QUANTITATIVE INTERPRETATION OF THERMAL NEUTRON DECAY TIME LOGS. *JPT, Journal of Petroleum Technology*, *23*, 743–763. https://doi.org/10.2118/2658-a-pa

Daukoru, J. W. (1975). PD 4(1) Petroleum Geology of the Niger Delta. *World Petroleum Congress*.

Doust, H. (1990). Petroleum geology of the Niger Delta. *Geological Society, London, Special Publications*, *50*(1), 365.

Doust, H., & Omatsola, E. (1990). Niger Delta. In *Divergent / Passive Margin Basins* (Vol. 48, pp. 201–238).

Eberhart-Phillips, D., Han, D.-H., & Zoback, M. D. (1989). Empirical relationships among seismic velocity, effective pressure, porosity, and clay content in sandstone. *Geophysics*, *54*(1), 82–89.

Elverhøi, A., & Rønningsland, T. M. (1978). Semiquantitative calculation of the relative amounts of kaolinite and chlorite by X-ray diffraction. *Marine Geology*, *27*(1–2), M19–M23.

Essien, U. E. (2019). Shale volume and porosity delineation of coast swamp depobelt in Niger Delta Region, Nigeria, Using Well Log. *International Journal of Advanced Geosciences*, *7*(2), 142–146.

Evamy, B. D., Haremboure, J., Kamerling, P., Knaap, W. A., Molloy, F. A., & Rowlands, P. H. (1978). Hydrocarbon habitat of Tertiary Niger delta. *AAPG Bulletin*, *62*(1), 1–39.

Fajana, A. O. (2021). Analytical modeling of effect of volume of shale different calculation methods on reservoir petrophysical parameters. *Earth Science Informatics*, *14*(1), 543–561.

Gardner, G. H. F., Gardner, L. W., & Gregory, Ar. (1974). Formation velocity and density—The diagnostic basics for stratigraphic traps. *Geophysics*, *39*(6), 770–780.

Kennedy, D. (2021). Gamma Ray Index-Shale Volume Transforms. *SPWLA 62nd Annual Logging Symposium*.

Kowallis, B. J., Jones, L. E. A., & Wang, H. F. (1984). Velocity-porosity-clay content systematics of poorly consolidated sandstones. *Journal of Geophysical Research: Solid Earth*, *89*(B12), 10355–10364.

Larionov, V. V. (1969). Borehole radiometry. *Nedra, Moscow*, *127*.

McPhee, C., Reed, J., & Zubizarreta, I. (2015). Wellsite Core Acquisition, Handling and Transportation. In *Developments in Petroleum Science* (Vol. 64, pp. 17–88). Elsevier. https://doi.org/10.1016/B978-0-444-63533-4.00002-0

Miranda-Trevino, J. C., & Coles, C. A. (2003). Kaolinite properties, structure and influence of metal retention on pH. *Applied Clay Science*, *23*(1–4), 133–139.

Oloruntobi, O., & Butt, S. (2019a). The new formation bulk density predictions for siliciclastic rocks. *Journal of Petroleum Science and Engineering*, *180*, 526–537. https://doi.org/10.1016/j.petrol.2019.05.017

Oloruntobi, O., & Butt, S. (2019b). The new formation bulk density predictions for siliciclastic rocks. *Journal of Petroleum Science and Engineering*, *180*, 526–537. https://doi.org/10.1016/j.petrol.2019.05.017

Oloruntobi, O., & Butt, S. (2019c). The new formation bulk density predictions for siliciclastic rocks. *Journal of Petroleum Science and Engineering*, *180*, 526–537. https://doi.org/10.1016/j.petrol.2019.05.017

Oloruntobi, O., & Butt, S. (2020). Application of specific energy for lithology identification. *Journal of Petroleum Science and Engineering*, *184*, 106402.

Oloruntobi, O., Falugba, O., Ekanem-Attah, O., Awa, C., & Butt, S. (2020). The Niger Delta basin fracture pressure prediction. *Environmental Earth Sciences*, *79*(13), 1–11.

Oyeyemi, K. D., Olowokere, M. T., & Aizebeokhai, A. P. (2019). Prospect analysis and hydrocarbon reservoir volume estimation in an exploration field, shallow offshore depobelt, Western Niger Delta, Nigeria. *Natural Resources Research*, *28*(1), 173–185.

Pauling, L. (1930). The structure of the chlorites. *Proceedings of the National Academy of Sciences*, *16*(9), 578–582.

Poupon, A., & Gaymard, R. (1970). The evaluation of clay content from logs. *SPWLA 11th Annual Logging Symposium*.

Poupon, A., & Levaux, J. (1971). *Evaluation of water saturation in shaly formations Proceeding of SPWLA 12th Annual Logging Symposium*.

Poupon, A., Loy, M. E., & Tixier, M. P. (1954). A contribution to electrical log interpretation in shaly sands. *Journal of Petroleum Technology*, *6*(06), 27–34.

Prasse, E., Hornbrook, J., Dharanidharan, B., Al-Bahar, M., Al-Sane, A., Bora, A., Shrinivisan, A., & Dhote, P. (2019). Clay Volume Is Not Shale Volume–A Case Study In The Miocene Lower Fars Formation in Kuwait. *SPE Kuwait Oil & Gas Show and Conference*.

Revil, A., & Cathles Iii, L. M. (1999). Permeability of shaly sands. *Water Resources Research*, *35*(3), 651–662.

Sayers, C. M., & den Boer, L. D. (2021). Porosity variation of elastic wave velocities in clean sandstones. *Geophysical Prospecting*, *69*(8–9), 1733–1744.

Schön, J. H. (2015). Electrical Properties. In *Developments in Petroleum Science* (Vol. 65, pp. 301–367). Elsevier B.V. https://doi.org/10.1016/B978-0-08-100404-3.00008-1

Schon, J. H., & Georgi, D. (2003). Dispersed shale, shaly-sand permeability-a hydraulic analog to the waxman-smits equation. *SPWLA 44th Annual Logging Symposium*.

Serra, O. (1984). *The Acquisition of Logging Data: Part A*. Elsevier.

Short, K. C., & Stauble, A. J. (1967). Outline of Geology of Niger Delta. *The American Association of Petroleum Geologists Bulletin*, *51*(5), 761–779.

Simandoux, P. (1963). Dielectric measurements on porous media, application to the measurements of water saturation: study of behavior of argillaceous formations. *Revue de l'Institut Francais Du Petrol*, *18*(suppl), 93–215.

Stieber, S. J. (1970). Pulsed neutron capture log evaluation-Louisiana gulf coast. *Fall Meeting of the Society of Petroleum Engineers of AIME*.

Szabó, N. P. (2011). Shale volume estimation based on the factor analysis of well-logging data. *Acta Geophysica*, *59*(5), 935–953.

Tuttle, M. L., Charpentier, R. R., & Brownfield, M. E. (1999). *The Niger Delta Petroleum System: Niger Delta Province, Nigeria, Cameroon, and Equatorial Guinea, Africa*. US Department of the Interior, US Geological Survey.

Winsauer, W. O., & McCardell, W. M. (1953). Ionic double-layer conductivity in reservoir rock. *Journal of Petroleum Technology*, *5*(05), 129–134.

Xu, S., & White, R. E. (1995). A new velocity model for clay-sand mixtures 1. *Geophysical Prospecting*, *43*(1), 91–118.

Yusuf, B., Oloruntobi, O., & Butt, S. (2019). The formation bulk density prediction for intact and fractured siliciclastic rocks. *Geodesy and Geodynamics*, *10*(6), 446–454.

Appendix A: Well Data

Table A-1

Well Data for Correlation Development and Validation

Well ID	Terrain	Measured Depth of Core Used for XRD (ft)	Measured Depth of Gamma Ray Reading Used for GRI (ft)	GRI (fraction)	Shale Volume from XRD (fraction)	Major Clay Mineral Content	Remarks
1	Swamp	9783	9783	0.864	0.7	Kaolinite (74%)	Correlation A
		10127	10127	0.891	0.81	Chlorite (50%)	Correlation B
2		8933	8933	0.876	0.621	Chlorite (71%)	Correlation B
3	Land	5110	5110	0.430	0.32	Kaolinite (92%)	Correlation A
4	Swamp	12944	12944	0.717	0.598	Kaolinite (78.7%)	Correlation A
6		11000	11000	0.863	0.64	Kaolinite (75%)	Correlation A
6		12950	12950	0.660	0.44	Kaolinite (59%)	Correlation A
7		10000	10000	0.602	0.52	Kaolinite (79%)	Correlation A
8		8240	8240	0.405	0.34	Chlorite (100%)	Correlation B
		9860	9860	0.621	0.59	Kaolinite (74.6%)	Correlation A
		12500	12500	0.715	0.62	Kaolinite (66.0%)	Correlation A
		12152	12152	0.663	0.57	Kaolinite (75%)	Correlation A
9		12156	12156	0.676	0.57	Kaolinite (74%)	Correlation A
		12443	12443	0.754	0.69	Kaolinite (68.1%)	Correlation A
11	Land	13690	13690	0.147	0.11	Kaolinite (64.0%)	Correlation A
		10500	10500	0.889	0.6	Kaolinite (70.0%)	Correlation A
12		11700	11700	0.800	0.55	Kaolinite (70.9%)	Correlation A
		12600	12600	0.940	0.68	Kaolinite (71.0%)	Correlation A
13		12020	12020	0.904	0.68	Kaolinite (71.0%)	Correlation A
		11990	11990	0.799	0.57	Kaolinite (70.0%)	Correlation A
14		12980	12980	0.963	0.55	Kaolinite (82.6%)	Correlation A
		13700	13700	0.166	0.07	Kaolinite (71.4%)	Correlation A
15		12800	12800	0.726	0.63	Kaolinite (73.0%)	Correlation A
16		15010	15010	0.470	0.32	Kaolinite (53.1%)	Correlation A
17	Swamp	9590	9590	0.549	0.22	Kaolinite (44.0%)	Correlation A
		9907	9907	0.506	0.16	Kaolinite (46.0%)	Correlation A
		10225	10225	0.698	0.25	Kaolinite (57.0%)	Correlation A
18	Land	7078.7	7078.7	0.478	0.23	Kaolinite (70%)	Correlation A
19	Swamp	6420.5	6420.5	0.210	0.18	Kaolinite (81%)	Correlation A

20		6941	6941	0.704	0.42	Kaolinite (70%)	Correlation A
21		6548	6548	0.433	0.23	Kaolinite (69%)	Correlation A
		6210	6210	0.744	0.72	Kaolinite (71%)	Correlation A
		6327	6327	0.680	0.55	Kaolinite (65%)	Correlation A
22		6635	6635	0.845	0.73	Kaolinite (84%)	Correlation A
		8781	8781	0.750	0.62	Kaolinite (69%)	Correlation A
		11155	11155	0.690	0.72	Kaolinite (66%)	Correlation A
		11336	11336	0.931	0.53	Chlorite (64%)	Correlation B
		9517	9517	0.774	0.706	Kaolinite (79.6%)	Correlation A
23	Land	9518.5	9518.5	0.712	0.706	Kaolinite (79.6%)	Correlation A
		9520	9520	0.754	0.706	Kaolinite (79.6%)	Correlation A
24		15170	15170	0.504	0.25	Kaolinite (76.0%)	Correlation A
		10325	10325	0.638	0.544	Kaolinite (87.7%)	Correlation A
		10325.5	10325.5	0.662	0.544	Kaolinite (87.7%)	Correlation A
		10326	10326	0.709	0.544	Kaolinite (87.7%)	Correlation A
25		10326.5	10326.5	0.763	0.544	Kaolinite (87.7%)	Correlation A
		10327	10327	0.736	0.544	Kaolinite (87.7%)	Correlation A
		10327.5	10327.5	0.713	0.544	Kaolinite (87.7%)	Correlation A
		10328	10328	0.692	0.544	Kaolinite (87.7%)	Correlation A
		7822	7822	0.801	0.666	Kaolinite (90.8%)	Correlation A
		7822.5	7822.5	0.853	0.666	Kaolinite (90.8%)	Correlation A
26		9650	9650	0.780	0.687	Kaolinite (67.6%)	Correlation A
		9650.5	9650.5	0.796	0.687	Kaolinite (67.6%)	Correlation A
		9651	9651	0.758	0.687	Kaolinite (67.6%)	Correlation A
27		10056	10056	0.239	0.05	Kaolinite (67%)	Correlation A
28		4609	4609	0.250	0.17	Kaolinite (67%)	Correlation A
		8520	8520	0.305	0.23	Kaolinite (36%)	Correlation A
		8564	8564	0.151	0.12	Kaolinite (66%)	Correlation A
29	Swamp	8611	8611	0.251	0.18	Kaolinite (53%)	Correlation A
		8700	8700	0.379	0.25	Kaolinite (50%)	Correlation A
		8772	8772	0.334	0.12	Kaolinite (52%)	Correlation A
		8882	8882	0.243	0.2	Kaolinite (56%)	Correlation A
30		6990	6990	0.799	0.56	Chlorite (80%)	Correlation B
		9270	9270	0.771	0.69	Chlorite (64%)	Correlation B
31		10056	10056	0.884	0.67	Chlorite (64%)	Correlation B
		6352	6352	0.963	0.73	Chlorite (74%)	Correlation B
		8834	8834	0.540	0.39	Mica (79%)	Not used
		4975	4975	0.751	0.472	Chlorite (76.9%)	Correlation B
		5382	5382	0.740	0.57	Chlorite (76.5%)	Correlation B
32		5800	5800	0.832	0.673	Kaolinite (70.7%)	Correlation A
		6165	6165	0.715	0.59	Kaolinite (80.6%)	Correlation A
		6800	6800	0.707	0.511	Kaolinite (75.8%)	Correlation A
		8036	8036	0.806	0.628	Kaolinite (72.2%)	Correlation A
33		9775	9775	0.756	0.655	Chlorite (70.8%)	Correlation A
		5750	5750	0.773	0.579	Kaolinite (88.7%)	Correlation A
34	Land	13990	13990	0.516	0.13	Kaolinite (64.0%)	Correlation A
14		13700	13700	0.166	0.07	Kaolinite (71.4%)	Validation
19	Swamp	8756	8756	0.225	0.2	Kaolinite (61%)	Validation
29	Swamp	8957	8957	0.247	0.17	Kaolinite (72%)	Validation

5	Swamp	15729	15729	0.276	0.16	Kaolinite (100%)	Validation
19	Swamp	8756	8756	0.371	0.2	Kaolinite (61%)	Validation
	Swamp	9559	9559	0.459	0.22	Kaolinite (46%)	Validation
17	Swamp	10284	10284	0.562	0.28	Kaolinite (65%)	Validation
	Swamp	10270	10270	0.700	0.47	Kaolinite (56%)	Validation
		9519	9519	0.717	0.706	Kaolinite (79.6%)	Validation
23		9518	9518	0.728	0.706	Kaolinite (79.6%)	Validation
	Land	9519.5	9519.5	0.737	0.706	Kaolinite (79.6%)	Validation
10		12133	12133	0.746	0.57	Kaolinite (59%)	Validation
23		9517.5	9517.5	0.755	0.706	Kaolinite (79.6%)	Validation
2	Swamp	8934	8934	0.804	0.621	Chlorite (71.0%)	Validation
1		9780	9780	0.840	0.65	Chlorite (64%)	Validation
33	Swamp	12000	12000	0.882	0.474	Kaolinite (92.7%)	Validation
12	Land	12600	12600	0.940	0.68	Kaolinite (71.0%)	Validation

Appendix B: Shale Specimen Mineralogy

Table B-1

Whole Rock Mineralogy from XRD Results

Well ID	Depth (ftah)	Clay Minerals	Quartz	Pyrite	Siderite	Feldspar	Zeolite	Gypsum	Calcite/ Dolomite	Sylvite	Jarosite	Plagioclase	Halite
Well 1	9780	65	28	0	0	8	0	0	0	0	0	0	0
Well 1	9783	70	23	0	0	7	0	0	0	0	0	0	0
Well 1	10127	81	12	0	0	7	0	0	0	0	0	0	0
Well 2	8933	62.1	32.7	3.3	0	1.9	0	0	0	0	0	0	0
Well 2	8934	62.1	32.7	3.3	0	1.9	0	0	0	0	0	0	0
Well 3	5110	32	51	0	0	17	0	0	0	0	0	0	0
Well 4	12944	59.8	30	1.5	4	4.7	0	0	0	0	0	0	0
Well 5	15729	16	43	0	0	0	0	0	37	0	0	0	4
Well 6	11000	64	24	1	1	3	0	1	1	0	1	4	0
Well 6	12950	44	38	1	1	10	0	0	0	0	1	5	5
Well 7	10000	52	27	2	3	7	0	0	6	0	0	3	0
Well 8	8240	42	53	0	0	8	0	0	7	0	0	0	0
Well 8	9860	59	28	1	1	6	0	1	0	0	0	4	0
Well 8	12500	62	25	1	1	9	0	0	0	0	0	2	0
Well 9	12443	69	23	1	0	3	0	0	0	0	1	3	0
Well 9	12152	57	22	2	4	5	0	3	5	0	0	2	0
Well 9	12156	57	28	2	2	4	0	2	3	0	0	2	0
Well 10	12133	56	19	1	1	5	0	2	3	0	8	5	0
Well 11	13690	11	71	0	0	4	0	0	10	0	0	1	3
Well 12	10500	60	25	1	3	5	0	2	1	0	0	3	0
Well 12	11700	55	24	2	3	8	0	1	3	0	0	3	1
Well 12	12600	68	20	1	3	4	0	1	2	0	0	1	0
Well 13	12020	68	14	2	3	4	0	0	4	0	0	2	3
Well 14	11990	57	24	2	5	5	0	0	3	0	0	2	2
Well 14	12980	23	68	1	2	3	0	0	2	0	0	1	0
Well 14	13700	7	87	0	1	2	0	0	2	0	0	1	0

Well 15	12800	63	21	2	3	5	0	0	5	0	0	1	0
Well 16	15010	32	47	4	1	5	0	0	6	0	0	0	0
Well 17	9559	22	51	7	7	13	0	0	0	0	0	0	0
Well 17	9907	16	37	11	28	8	0	0	0	0	0	0	0
Well 17	9590	22	56	7	8	7	0	0	0	0	0	0	0
Well 17	10284	28	44		14	14	0	0	0	0	0	0	0
Well 17	10225	25	43	4	15	13	0	0	0	0	0	0	0
Well 17	10270	47	36	4	8	5	0	0	0	0	0	0	0
Well 18	7079	23	54		16	7	0	0	0	0	0	0	0
Well 19	6421	18	59	6	0	17	0	0	0	0	0	0	0
Well 19	8756	20	37	5	18	0	20	0	0	0	0	0	0
Well 20	6941	42	40	6	0	12	0	0	0	0	0	0	0
Well 21	6548	23	62	2	7	3	0	0	0	0	0	0	0
Well 22	6210	72	19	0	0	9	0	0	0	0	0	0	0
Well 22	6327	55	35	0	0	20	0	0	0	0	0	0	0
Well 22	6635	73	20	0	0	7	0	0	0	0	0	0	0
Well 22	8781	62	29	0	0	9	0	0	0	0	0	0	0
Well 22	11155	72	16	0	0	12	0	0	0	0	0	0	0
Well 22	11336	53	38	0	0	9	0	0	0	0	0	0	0
Well 23	9519	70.6	20.2	0	4.6	4.6	0	0	0	0	0	0	0
Well 23	9519	70.6	20.2	0	4.6	4.6	0	0	0	0	0	0	0
Well 23	9518	70.6	20.2	0	4.6	4.6	0	0	0	0	0	0	0
Well 23	9520	70.6	20.2	0	4.6	4.6	0	0	0	0	0	0	0
Well 23	9520	70.6	20.2	0	4.6	4.6	0	0	0	0	0	0	0
Well 23	9518	70.6	20.2	0	4.6	4.6	0	0	0	0	0	0	0
Well 23	9517	70.6	20.2	0	4.6	4.6	0	0	0	0	0	0	0
Well 24	15170	21	33	6	0	6	0	0	28	0	0	0	6
Well 25	10325	54.4	21.9	0	15.6	8.1	0	0	0	0	0	0	0
Well 25	10326	54.4	21.9	0	15.6	8.1	0	0	0	0	0	0	0
Well 25	10328	54.4	21.9	0	15.6	8.1	0	0	0	0	0	0	0
Well 25	10326	54.4	21.9	0	15.6	8.1	0	0	0	0	0	0	0
Well 25	10328	54.4	21.9	0	15.6	8.1	0	0	0	0	0	0	0
Well 25	10327	54.4	21.9	0	15.6	8.1	0	0	0	0	0	0	0
Well 25	10327	54.4	21.9	0	15.6	8.1	0	0	0	0	0	0	0
Well 26	9651	68.7	22.7	7	0	1.6	0	0	0	0	0	0	0
Well 26	9650	68.7	22.7	7	0	1.6	0	0	0	0	0	0	0
Well 26	7822	66.6	28.3	0	3.1	2	0	0	0	0	0	0	0
Well 26	7823	66.6	28.3	0	3.1	2	0	0	0	0	0	0	0
Well 27	10056	5	52	0	12	31	0	0	0	0	0	0	0
Well 28	4609	17	69	4	0	10	0	0	0	0	0	0	0
Well 29	8564	12	20	5	6	2	0	55	0	0	0	0	0
Well 29	8882	20	43	4	6	27	0	0	0	0	0	0	0
Well 29	8957	17	50	0	17	16	0	0	0	0	0	0	0
Well 29	8611	18	42	11	22	7	0	0	0	0	0	0	0
Well 29	8520	23	64	4	0	9	0	0	0	0	0	0	0
Well 29	8772	12	36	4	13	35	0	0	0	0	0	0	0
Well 29	8700	25	25	13	14	23	0	0	0	0	0	0	0
Well 30	10056	67	33	0	0	0	0	0	0	0	0	0	0
Well 30	9270	69	31	0	0	0	0	0	0	0	0	0	0

Well 30	6990	56	38	0	0	20	0	0	0	0	0	0	0
Well 31	8834	39	49	0	0	12	0	0	0	0	0	0	0
Well 31	6352	73	22	0	0	5	0	0	0	0	0	0	0
Well 32	6800	51.1	36	0	9.1	3.8	0	0	0	0	0	0	0
Well 32	4975	47.2	39.4	0	9.7	3.7	0	0	0	0	0	0	0
Well 32	6165	59	21.7	0	16.7	2.6	0	0	0	0	0	0	0
Well 32	5382	57	38	4	0	1.1	0	0	0	0	0	0	0
Well 32	9775	65.5	28.4	3.9	0	2.2	0	0	0	0	0	0	0
Well 32	8036	62.8	30.2	4.3	1.1	1.6	0	0	0	0	0	0	0
Well 32	5800	67.3	27.2	0	0	5.5	0	0	0	0	0	0	0
Well 33	5750	57.9	39.3	0	2.8	0	0	0	0	0	0	0	0
Well 33	12000	47.4	44.2	2.2	3.7	2.5	0	0	0	0	0	0	0
Well 34	13990	13	74	1	1	2	0	0	7	1	0	1	0
	AVERAGE	**48.2**	**33.5**	**1.9**	**5.0**	**7.2**	**0.2**	**0.8**	**1.5**	**0.0**	**0.1**	**0.5**	**0.3**

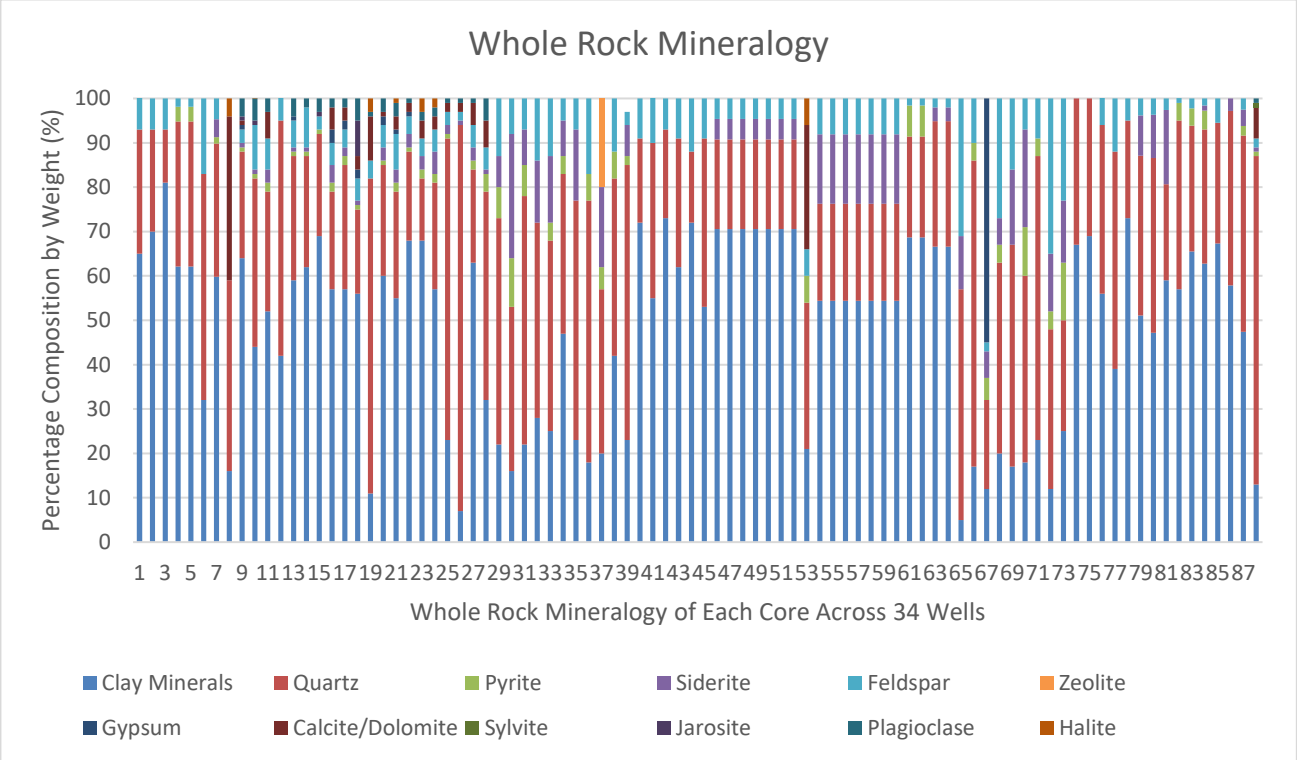

Table B-2

Clay Mineral Composition by % Weight

Well ID	Chlorite	Kaolinite	Mica	Mica/ Smectite (M-sm)	Smectite (Sm)	Vermiculite	Illite	Mica-Vermiculite (M/V)	Illite/Mica	Chlorite-Mica	Chlorite - Smectite	Mx Ilite/Smectite
Well 1	64.0	13.0	0.0	23.0	0.0	0.0	0.0	0.0	0.0	0.0	0.0	0.0
Well 1	0.0	74.0	3.0	23.0	0.0	0.0	0.0	0.0	0.0	0.0	0.0	0.0
Well 1	50.0	0.0	35.0	0.0	0.0	0.0	15.0	0.0	0.0	0.0	0.0	0.0
Well 2	71.0	0.0	8.5	0.0	0.0	0.0	0.0	0.0	0.0	20.5	0.0	0.0
Well 2	71.0	0.0	8.5	0.0	0.0	0.0	0.0	0.0	0.0	20.5	0.0	0.0
Well 3	0.0	92.0	0.0	0.0	0.0	0.0	0.0	0.0	0.0	0.0	0.0	0.0
Well 4	0.0	78.7	21.3	0.0	0.0	0.0	0.0	0.0	0.0	0.0	0.0	0.0
Well 5	0.0	100.0	0.0	0.0	0.0	0.0	0.0	0.0	0.0	0.0	0.0	0.0
Well 6	6.0	75.0	0.0	0.0	0.0	0.0	0.0	0.0	5.0	0.0	0.0	14.0
Well 6	16.0	59.0	0.0	0.0	0.0	0.0	0.0	0.0	16.0	0.0	0.0	9.0
Well 7	4.0	79.0	0.0	0.0	0.0	0.0	0.0	0.0	2.0	0.0	0.0	15.0
Well 8	100.0	0.0	0.0	0.0	0.0	0.0	0.0	0.0	0.0	0.0	0.0	0.0
Well 8	8.5	74.6	0.0	0.0	0.0	0.0	0.0	0.0	6.8	0.0	0.0	10.2
Well 8	11.0	66.0	0.0	0.0	0.0	0.0	0.0	0.0	10.0	0.0	0.0	13.0
Well 9	8.7	68.1	0.0	0.0	0.0	0.0	0.0	0.0	11.6	0.0	0.0	11.6
Well 9	9.0	75.0	0.0	0.0	0.0	0.0	0.0	0.0	2.0	0.0	0.0	14.0
Well 9	11.0	74.0	0.0	0.0	0.0	0.0	0.0	0.0	4.0	0.0	0.0	12.0
Well 10	7.0	59.0	0.0	0.0	0.0	0.0	0.0	0.0	29.0	0.0	0.0	5.0
Well 11	18.0	64.0	0.0	0.0	0.0	0.0	0.0	0.0	0.0	0.0	0.0	18.0
Well 12	8.3	70.0	0.0	0.0	0.0	0.0	0.0	0.0	5.0	0.0	0.0	16.7
Well 12	9.1	70.9	0.0	0.0	0.0	0.0	0.0	0.0	5.5	0.0	0.0	14.5
Well 12	18.0	71.0	0.0	0.0	0.0	0.0	0.0	0.0	4.0	0.0	0.0	7.0
Well 13	13.0	71.0	0.0	0.0	0.0	0.0	0.0	0.0	6.0	0.0	0.0	10.0
Well 14	9.0	70.0	0.0	0.0	0.0	0.0	0.0	0.0	5.0	0.0	0.0	16.0
Well 14	4.3	82.6	0.0	0.0	0.0	0.0	0.0	0.0	8.7	0.0	0.0	4.3
Well 14	14.3	71.4	14.3	0.0	0.0	0.0	0.0	0.0	0.0	0.0	0.0	0.0
Well 15	6.0	73.0	0.0	0.0	0.0	0.0	0.0	0.0	5.0	0.0	0.0	16.0
Well 16	12.5	53.1	0.0	0.0	0.0	0.0	0.0	0.0	6.3	0.0	0.0	28.1
Well 17	0.0	46.0	0.0	48.0	6.0	0.0	0.0	0.0	0.0	0.0	0.0	0.0
Well 17	0.0	44.0	0.0	44.0	12.0	0.0	0.0	0.0	0.0	0.0	0.0	0.0
Well 17	0.0	65.0	7.0	28.0	0.0	0.0	0.0	0.0	0.0	0.0	0.0	0.0
Well 17	0.0	65.0	35.0	0.0	0.0	0.0	0.0	0.0	0.0	0.0	0.0	0.0
Well 17	0.0	57.0	0.0	0.0	0.0	0.0	0.0	43.0	0.0	0.0	0.0	0.0
Well 17	0.0	56.0	0.0	44.0	0.0	0.0	0.0	0.0	0.0	0.0	0.0	0.0
Well 18	0.0	70.0	0.0	23.0	7.0	0.0	0.0	0.0	0.0	0.0	0.0	0.0
Well 19	0.0	81.0	0.0	0.0	19.0	0.0	0.0	0.0	0.0	0.0	0.0	0.0
Well 19	0.0	61.0	0.0	32.0	7.0	0.0	0.0	0.0	0.0	0.0	0.0	0.0
Well 20	0.0	70.0	0.0	23.0	7.0	0.0	0.0	0.0	0.0	0.0	0.0	0.0
Well 21	0.0	69.0	0.0	0.0	31.0	0.0	0.0	0.0	0.0	0.0	0.0	0.0
Well 22	0.0	71.0	0.0	0.0	0.0	0.0	3.0	26.0	0.0	0.0	0.0	0.0
Well 22	0.0	65.0	7.0	0.0	0.0	0.0	0.0	28.0	0.0	0.0	0.0	0.0
Well 22	0.0	84.0	7.0	0.0	0.0	0.0	9.0	0.0	0.0	0.0	0.0	0.0
Well 22	0.0	69.0	8.0	0.0	0.0	0.0	3.0	0.0	0.0	0.0	0.0	20.0
Well 22	0.0	66.0	3.0	0.0	0.0	0.0	0.0	31.0	0.0	0.0	0.0	0.0
Well 22	64.0	0.0	8.0	0.0	0.0	0.0	0.0	0.0	0.0	0.0	0.0	28.0
Well 23	0.0	79.6	7.6	11.1	1.7	0.0	0.0	0.0	0.0	0.0	0.0	0.0
Well 23	0.0	79.6	7.6	11.1	1.7	0.0	0.0	0.0	0.0	0.0	0.0	0.0
Well 23	0.0	79.6	7.6	11.1	1.7	0.0	0.0	0.0	0.0	0.0	0.0	0.0

Well 23	0.0	79.6	7.6	11.1	1.7	0.0	0.0	0.0	0.0	0.0	0.0	0.0
Well 23	0.0	79.6	7.6	11.1	1.7	0.0	0.0	0.0	0.0	0.0	0.0	0.0
Well 23	0.0	79.6	7.6	11.1	1.7	0.0	0.0	0.0	0.0	0.0	0.0	0.0
Well 23	0.0	79.6	7.6	11.1	1.7	0.0	0.0	0.0	0.0	0.0	0.0	0.0
Well 24	0.0	76.0	24.0	0.0	0.0	0.0	0.0	0.0	0.0	0.0	0.0	0.0
Well 25	0.0	87.7	12.3	0.0	0.0	0.0	0.0	0.0	0.0	0.0	0.0	0.0
Well 25	0.0	87.7	12.3	0.0	0.0	0.0	0.0	0.0	0.0	0.0	0.0	0.0
Well 25	0.0	87.7	12.3	0.0	0.0	0.0	0.0	0.0	0.0	0.0	0.0	0.0
Well 25	0.0	87.7	12.3	0.0	0.0	0.0	0.0	0.0	0.0	0.0	0.0	0.0
Well 25	0.0	87.7	12.3	0.0	0.0	0.0	0.0	0.0	0.0	0.0	0.0	0.0
Well 25	0.0	87.7	12.3	0.0	0.0	0.0	0.0	0.0	0.0	0.0	0.0	0.0
Well 25	0.0	87.7	12.3	0.0	0.0	0.0	0.0	0.0	0.0	0.0	0.0	0.0
Well 26	0.0	67.6	20.2	0.0	0.7	0.0	0.0	0.0	0.0	0.0	0.0	11.5
Well 26	0.0	67.6	20.2	11.5	0.7	0.0	0.0	0.0	0.0	0.0	0.0	0.0
Well 26	0.0	90.8	9.2	0.0	0.0	0.0	0.0	0.0	0.0	0.0	0.0	0.0
Well 26	0.0	90.8	9.2	0.0	0.0	0.0	0.0	0.0	0.0	0.0	0.0	0.0
Well 27	0.0	67.0	33.0	0.0	0.0	0.0	0.0	0.0	0.0	0.0	0.0	0.0
Well 28	0.0	67.0	0.0	33.0	0.0	0.0	0.0	0.0	0.0	0.0	0.0	0.0
Well 29	0.0	66.0	0.0	0.0	0.0	0.0	0.0	34.0	0.0	0.0	0.0	0.0
Well 29	0.0	56.0	0.0	0.0	0.0	0.0	0.0	44.0	0.0	0.0	0.0	0.0
Well 29	0.0	72.0	0.0	0.0	0.0	0.0	0.0	28.0	0.0	0.0	0.0	0.0
Well 29	0.0	53.0	0.0	0.0	0.0	0.0	0.0	47.0	0.0	0.0	0.0	0.0
Well 29	0.0	36.0	5.0	0.0	0.0	0.0	0.0	59.0	0.0	0.0	0.0	0.0
Well 29	0.0	52.0	0.0	0.0	0.0	0.0	0.0	48.0	0.0	0.0	0.0	0.0
Well 29	0.0	50.0	0.0	0.0	0.0	0.0	0.0	50.0	0.0	0.0	0.0	0.0
Well 30	64.0	0.0	36.0	0.0	0.0	0.0	0.0	0.0	0.0	0.0	0.0	0.0
Well 30	76.0	0.0	24.0	0.0	0.0	0.0	0.0	0.0	0.0	0.0	0.0	0.0
Well 30	80.0	4.0	16.0	0.0	0.0	0.0	0.0	0.0	0.0	0.0	0.0	0.0
Well 31	0.0	21.0	79.0	0.0	0.0	0.0	0.0	0.0	0.0	0.0	0.0	0.0
Well 31	74.0	0.0	0.0	0.0	0.0	0.0	0.0	26.0	0.0	0.0	0.0	0.0
Well 32	0.0	75.8	5.7	16.4	2.1	0.0	0.0	0.0	0.0	0.0	0.0	0.0
Well 32	76.9	0.0	2.8	0.0	1.6	0.0	0.0	0.0	0.0	0.0	18.7	0.0
Well 32	0.0	80.6	11.7	0.0	7.7	0.0	0.0	0.0	0.0	0.0	0.0	0.0
Well 32	76.5	0.0	11.3	0.0	2.6	0.0	0.0	0.0	0.0	0.0	9.6	0.0
Well 32	70.8	0.0	11.6	0.0	0.0	0.0	0.0	0.0	0.0	0.0	17.6	0.0
Well 32	0.0	72.2	10.5	0.0	0.0	5.0	0.0	12.3	0.0	0.0	0.0	0.0
Well 32	0.0	70.7	4.5	19.9	4.9	0.0	0.0	0.0	0.0	0.0	0.0	0.0
Well 33	0.0	88.7	11.3	0.0	0.0	0.0	0.0	0.0	0.0	0.0	0.0	0.0
Well 33	0.0	92.7	7.3	0.0	0.0	0.0	0.0	0.0	0.0	0.0	0.0	0.0
Well 34	7.7	76.9	0.0	0.0	0.0	0.0	0.0	0.0	7.7	0.0	0.0	7.7
AVERAGE	**13.0**	**61.2**	**7.5**	**5.1**	**1.4**	**0.1**	**0.3**	**5.4**	**1.6**	**0.5**	**0.5**	**3.4**

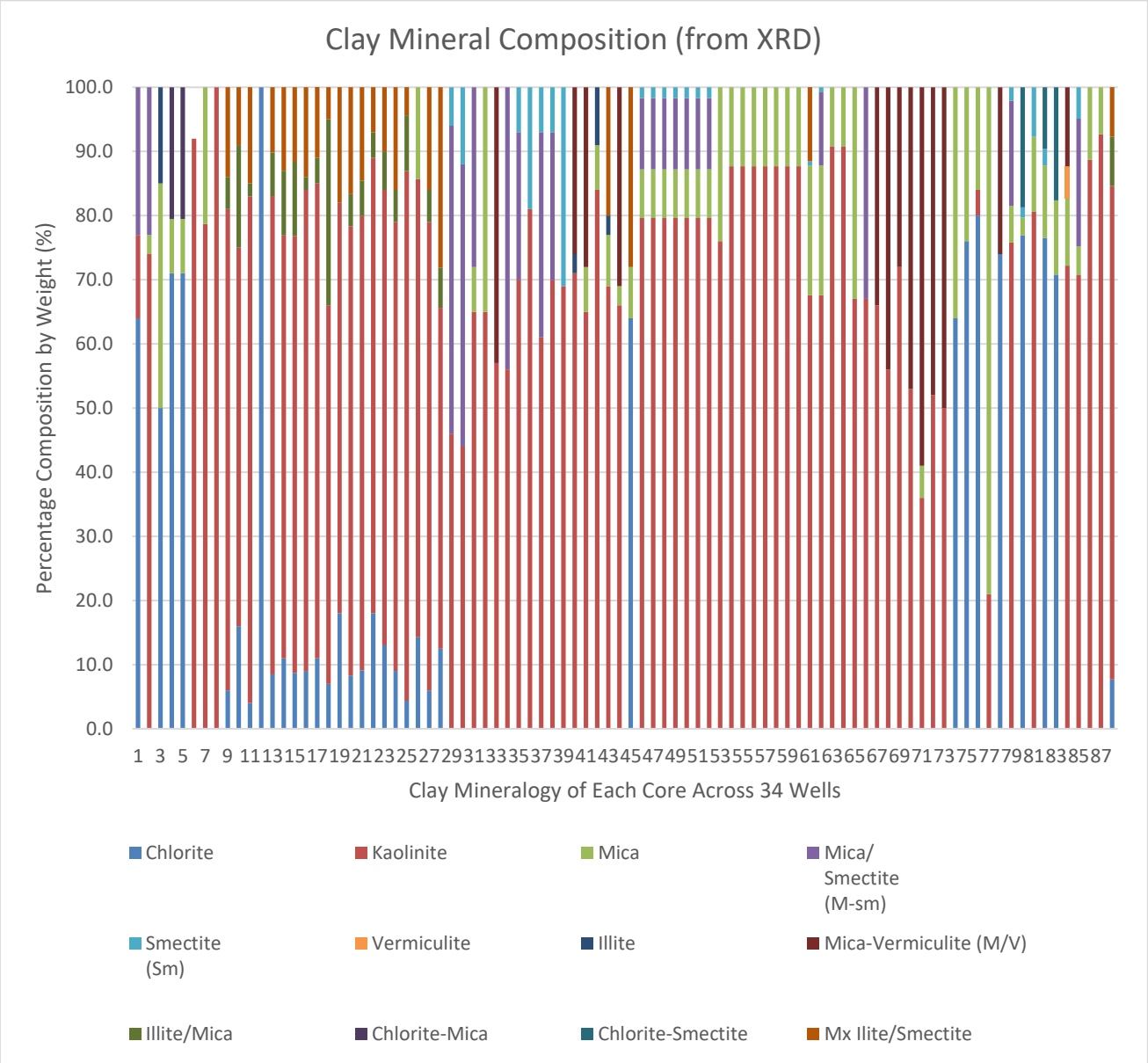
Clay Mineral Composition (from XRD)
Percentage Composition by Weight (%)
100.0
90.0
80.0
70.0
60.0
50.0
40.0
30.0
20.0
10.0
0.0
1 3 5 7 9 11 13 15 17 19 21 23 25 27 29 31 33 35 37 39 41 43 45 47 49 51 53 55 57 59 61 63 65 67 69 71 73 75 77 79 81 83 85 87
Clay Mineralogy of Each Core Across 34 Wells
Chlorite
Kaolinite
Mica
Mica/ Smectite (M-sm)
Smectite (Sm)
Vermiculite
Illite
Mica-Vermiculite (M/V)
Illite/Mica
Chlorite-Mica
Chlorite-Smectite
Mx Ilite/Smectite